8633

NACA TN 2210

TECH LIBRARY KAFB, NM
0065059

NATIONAL ADVISORY COMMITTEE FOR AERONAUTICS

TECHNICAL NOTE 2210

IMPACT-PRESSURE INTERPRETATION IN A RAREFIED GAS AT SUPERSONIC SPEEDS

By E. D. Kane and G. J. Maslach

University of California

Washington
October 1950

319.98/41

TECH LIBRARY KAFB, NM

0065059

NATIONAL ADVISORY COMMITTEE FOR AERONAUTICS

TECHNICAL NOTE 2210

IMPACT-PRESSURE INTERPRETATION IN A RAREFIED GAS AT SUPERSONIC SPEEDS

By E. D. Kane and G. J. Maslach

SUMMARY

The interpretation of measured impact pressures in a rarefied gas is reviewed and available analyses are summarized. Experimental results are presented for source-shaped impact tubes for Mach numbers between 2.3 and 3.6 and Reynolds numbers from 25 to 804. The data show that the Rayleigh formula requires correction for conditions where the ratio of Mach number to Reynolds number is greater than 0.015, where the Reynolds number is based on the impact-probe diameter and free-stream conditions. The maximum correction to the Rayleigh formula, obtained at the low pressure limit of the experimental equipment, was 13 percent (when the ratio of Mach number to Reynolds number was 0.093).

INTRODUCTION

One of the basic instrumentation techniques in aerodynamics involves insertion of a probe into the flow field and measurement of a pressure at an orifice or tap located at the probe surface. By means of an appropriate analysis for a given probe shape, or by direct calibration, the measured pressure can be related to certain properties of the gas flow. A common example of this procedure is the use of an impact or total-head tube which gives a pressure that is related to the Mach number and static pressure (reference 1, p. 77), or two equivalent quantities, by an analysis based on the assumption of a nonviscous, compressible fluid. This analysis fails when the viscous forces become appreciable compared with the inertia or pressure forces in the fluid; that is, when the Reynolds number becomes sufficiently small. The behavior of an impact tube in a viscous, incompressible fluid at low speeds was examined by Homann (reference 2). Recently, the analysis was extended to include compressiblity effects (reference 3), with the result that a measured impact pressure was found to be related to a Reynolds number in addition to the Mach number and static pressure. The conclusions of reference 3 were verified approximately by experimental work performed at subsonic speeds (reference 4). For a sufficiently rarefied gas, where continuum treatments

fail but the methods of kinetic theory are applicable, an analytical solution relating an impact pressure to free-stream conditions exists (reference 5) and has been verified partially in a molecular-beam apparatus (reference 6). No results have been available in the transition region between continuum and extremely rarefied (free-molecular) flow conditions.

The purpose of the experimental investigation summarized in the present report was to determine the magnitude and direction of deviations from the Rayleigh formula (reference 1, p. 77) for a source-shaped impact tube in a supersonic air flow at low Reynolds numbers. The experimental results are indicative of the effects to be expected for impact tubes used at high altitudes, or in supersonic or hypersonic wind tunnels producing rarefied-gas streams.

This work was conducted at the University of California under the sponsorship and with the financial assistance of the National Advisory Committee for Aeronautics and was under the immediate supervision of Professors R. G. Folsom, E. D. Kane, and S. A. Schaaf of the Department of Engineering at Berkeley.

SYMBOLS

a	local sound speed in gas, consistent units
C	constant in equation (13), 202° F absolute
d	probe diameter, inches
K_1	constant defined in equations (2), (3), and (4)
M	Mach number (V/a)
p	gas pressure, microns of mercury
R	gas constant $(p/\rho T)$
Re	Reynolds number $(Vd\rho/\mu)$
S	speed ratio $\left(M\sqrt{\gamma/2}\right)$
T	gas temperature, °F absolute
T_o	stagnation or reservoir temperature, °F absolute
V	gas velocity, consistent units
y	variable in definite integral defining error function erf S

α, β, δ	constants
γ	ratio of specific heats (1.40 for air)
μ	gas viscosity, pounds per second per foot
ρ	gas density, consistent units
μ_o	gas viscosity at 450° F absolute (equation (13)), pounds per second per foot
ϕ_1	function defined in equations (2), (3), and (4)
ψ	dimensionless group defined by equation (14) of reference 7

Subscripts:

i	impact
s	static
1	conditions behind normal shock wave
2	quantity measured at surface of cone (probe 15)

SUMMARY OF AVAILABLE ANALYSES FOR IMPACT TUBES

The Rayleigh formula has been applied to interpretation of impact-pressure measurements under flow conditions where the assumptions of a nonviscous, compressible gas are applicable. The Rayleigh formula can be written (reference 1, p. 77)

$$\frac{p_i}{p_s} = \frac{\left(\frac{\gamma + 1}{2} M^2\right)^{\gamma/(\gamma-1)}}{\left(\frac{2\gamma}{\gamma + 1} M^2 - \frac{\gamma - 1}{\gamma + 1}\right)^{1/(\gamma-1)}} \tag{1}$$

and results from consideration of a stagnation line flow through a normal shock followed by an isentropic deceleration to zero velocity at the

stagnation point. Equation (1) indicates that the impact pressure is a function solely of the free-stream static pressure and Mach number.

Reference 3 retains the assumptions of a stagnation line flow through a normal shock wave but includes viscous effects in the subsonic flow field by means of a boundary-layer analysis. The result can be written

$$\frac{p_i}{p_s} = \left(\frac{p_i}{p_s}\right)_{\text{equation (1)}} + \left(\frac{2\gamma}{\gamma + 1} M^2 - \frac{\gamma - 1}{\gamma + 1}\right)\frac{\gamma M_1{}^2}{Re_1} \frac{\phi_1}{1 + \frac{K_1}{\sqrt{Re_1}}} \tag{2}$$

Equation (2) indicates that the measured impact pressure equals the impact pressure computed from equation (1), plus a "correction" term which becomes increasingly important as the Reynolds number decreases. The functions ϕ_1 and K_1 in equation (2) depend on the shape of the impact tube. For a full sphere, reference 3 gives

$$\left.\begin{aligned} \phi_1 &= 3 - \frac{83}{110} M_1{}^2 \\ K_1 &= 0.457 \end{aligned}\right\} \tag{3}$$

and for a hemisphere joined to a cylinder, reference 4 gives

$$\left.\begin{aligned} \phi_1 &= \frac{29}{8} - \frac{31}{34} M_1{}^2 \\ K_1 &= 0.457 \end{aligned}\right\} \tag{4}$$

Tsien (reference 8) pointed out that sufficiently high values of the Mach number and low values of the Reynolds number characterized entry into a regime of "slip" or transition flow and rendered theoretical treatments difficult by requiring consideration of a viscous, compressible fluid and by modifying boundary conditions. It would be expected, therefore, that equation (2), derived by a continuum fluid analysis, would become invalid for sufficiently small Reynolds numbers - that is,

for a sufficiently rarefied gas. Reference 8 suggested, as an order-of-magnitude estimate, that a continuum analysis might become invalid when $M/\sqrt{Re}$ is greater than approximately 0.01.

The methods of kinetic theory are applicable to interpretation of an impact tube in an extremely rarefied gas (M/Re is greater than approximately 10 according to reference 8). Reference 5 analyzes this situation and shows that an impact pressure measured in a reservoir at the end of a straight tube is related to the Mach number and static pressure in the free stream but also depends on the geometry (ratio of internal length to diameter) of the impact tube and the temperature ratio between free stream and reservoir. This theoretical result has been verified partially in a molecular-beam apparatus (reference 6).

In order to compare the free-molecular-flow analysis with equations (1) and (2), consider a special case of a spherical impact tube with a sharp-edged pressure orifice (fig. 1). This sphere diameter is sufficiently small compared with the gas molecular mean free path so that a shock wave will not occur. The internal baffle is provided so that molecules entering the orifice will strike a surface before entering the connection to the pressure-sensitive element (an assumption of the free-molecular-flow analysis). For conditions of figure 1, reference 5 gives the relation

$$\frac{p_i}{p_s} = \sqrt{\frac{T_i}{T_s}}\left[e^{-S^2} + S\sqrt{\pi}\,(1 + \operatorname{erf} S)\right] \tag{5}$$

where the speed ratio S is related to the Mach number M by

$$S = M\sqrt{\gamma/2}$$

and

$$\operatorname{erf} S = \frac{2}{\sqrt{\pi}}\int_0^S e^{-y^2}\,dy$$

The ratio T_i/T_s must be determined from heat-transfer considerations or measured as an additional quantity. For the purpose of this comparison between impact-tube formulas, the analysis of reference 7 can be used to approximate the temperature ratio T_i/T_s. For a flat plate

normal to the macroscopic flow direction, with the additional assumptions that radiation is absent and that the interior of the impact tube is insulated, the result is

$$S^2 + \psi + 1 - \frac{3T_i}{T_s} = 0 \tag{6}$$

where ψ is shown in figure 5, reference 7, as a function of S (or U/V_m in the nomenclature of that paper). Substituting equation (6) in equation (5) gives

$$\frac{p_i}{p_s} = \left[\frac{1}{3}\left(\frac{\gamma M^2}{2} + 1 + \psi\right)\right]^{1/2}\left[e^{-\frac{\gamma M^2}{2}} + M\sqrt{\frac{\gamma\pi}{2}}\left(1 + \operatorname{erf} M\sqrt{\frac{\gamma}{2}}\right)\right] \tag{7}$$

Equation (7) relates p_i/p_s to a function of M (or S) only and can be compared with equations (1) and (2) for air ($\gamma = 1.40$). The result is shown in figure 2, which indicates the status of theoretical information on interpretation of impact-tube readings in a rarefied gas at supersonic speeds.

Examination of figure 2 indicates a need for further experimental and theoretical investigation of the following problems:

(1) What are the limits of applicability of the Rayleigh formula (equation (1))? Can these limits be formulated in terms of the common flow parameters, Mach and Reynolds numbers?

(2) Is the analysis proposed by equation (2) valid? If so, within what limits - that is, for what degree of rarefaction?

(3) An improved experimental verification is needed for the results of reference 6 (of which equation (5) is a special case).

(4) Theoretical and experimental results are needed for the entire transition region, where it is known that neither the Rayleigh formula nor reference 3 is applicable.

(5) The effect of impact-probe geometry and angle of attack must be determined for all flow regimes.

The present report is concerned with an experimental investigation of the first two problems enumerated above, for a single-impact-tube geometry at zero angle of attack.

EXPERIMENTAL APPARATUS

All test work was performed in a low-density supersonic wind tunnel, known as the no. 3 wind tunnel, which is described in detail in reference 9. The two axisymmetric nozzles (2 and 3) that were used had diameters at the exit plane of $5\frac{1}{2}$ and $5\frac{1}{4}$ inches, respectively. Nozzle 2 gave Mach numbers from 2.3 to 2.8, while the range of nozzle 3 was from 2.8 to 3.6. The corresponding Reynolds number values extended from 170 (per inch characteristic dimension) for $M = 2.3$ to 930 for $M = 2.8$ with nozzle 2, and from 230 for $M = 2.8$ to 1830 per inch for $M = 3.6$ with nozzle 3. The design of nozzle 2 is covered in reference 10; that of nozzle 3, in reference 9.

Three impact tubes were used during this investigation (figs. 3 and 4). All tubes had source-shaped profiles and were geometrically similar throughout. The critical dimensions were: Outside diameters, 0.150, 0.300, and 0.600 inch with hole diameters of 0.030, 0.060, and 0.120 inch, respectively. The minimum-size (0.150-in. diameter) impact tube was selected on time-response considerations using the technique presented in reference 11. The maximum (0.600-in. diameter) was selected after evaluating the nature of the velocity distribution in the test section. The 0.300-inch-diameter impact tube had been used extensively previous to this investigation to determine flow conditions in nozzles 2 and 3. The three impact tubes permitted tests to be made for Reynolds numbers from 25 to 556 (based on impact-tube diameter) in nozzle 2 and permitted the Reynolds number range to be extended from 35 to 804 in nozzle 3.

A U-tube manometer (see fig. 5) filled with a low-vapor-pressure oil (butyl phthalate) was used to measure the impact pressures throughout the four runs. The reference leg of the manometer was connected to a pump system which maintained a pressure of approximately 0.1 micron of mercury, and the other leg was connected through flexible tubing to the impact tube mounted in the test section. Two optical elements have been incorporated into the manometer to help minimize reading errors and also to lessen eye fatigue. The image of the meniscus in the reference leg can be made to coincide with a cross hair on the right-hand screen. The left-hand screen then can be adjusted to bring the image of the meniscus in the left leg of the manometer into position by means of a micrometer screw. The impact pressure in inches of oil is then read using the scale and vernier on the micrometer screw. The least count of the manometer vernier is 0.001 inch and experience has shown that readings can be reproduced to ±0.0005 inch or approximately ±1 micron. The manometer was calibrated before and after each run to determine the manometer conversion and zero correction factor for that run. The primary instrument used in this procedure was a specially built McLeod gage, also

shown in figure 5. This gage, built with 3/16-inch inside-diameter glass tubing, measures a maximum pressure of 440 microns of mercury. The least count of the scale is 0.5 millimeter and estimates are made within this interval using the viewing telescope shown mounted on the gage frame. Analysis based on a ±0.25-millimeter reading error shows that the precision of this instrument is ±0.1 micron at 5 microns of mercury and ±1.0 micron at 400 microns of mercury. On the basis of calibrations made before and after each run, the pressure readings obtained with the oil manometer, which ranged from 250 to 1930 microns, should have an uncertainty less than ±3 microns of mercury.

The flow of gas into the wind tunnel was controlled by means of needle valves placed downstream from a gas flowmeter. The meter was a modified Fischer and Porter air Rotometer capable of measuring flows ranging from 1.5 to 15 pounds per hour. Two floats were contained within this instrument. Undesignated readings in table 1 apply to the smaller float, while the abbreviation LF refers to the larger float.

A static probe (15) consisting of a 5° half-angle cone joined to a 0.300-inch-diameter cylinder, with pressure orifices located on the cone surface, was used to determine the static pressure p_s. The use and interpretation of the pressure readings obtained with this probe are discussed in a later section of this report.

A traversing mechanism within the test section of the no. 3 wind tunnel (reference 9) provided means for mounting and moving models or probes in the test section. Motors mounted inside the vacuum chamber allowed remote operation of the traversing mechanism. Selsyn motors and generators gave position indication on standard five-place counters located outside the vacuum chamber at the control console. Two different probes could be mounted on the mechanism at one time, and either of the two probes moved into the test section as required without alteration of the air stream.

A flow-visualization technique, similar to that described in references 12 and 13, was employed to provide photographs indicating the position and character of shock waves associated with the probes used in this investigation.

EXPERIMENTAL PROCEDURE

The experimental procedure used throughout the tests was to measure the impact pressure for a fixed flow condition at the exit plane of a nozzle with two geometrically similar impact tubes. The flow conditions were not changed while one tube was withdrawn from and another tube was

placed into the air stream by the traversing mechanism. Therefore, the net effect of the tests was to measure comparative pressure readings of two impact probes in a fixed flow, each probe having a characteristic Reynolds number determined by the probe diameter. Two reasons can be given for using this comparison technique to observe Reynolds number effects on impact-tube behavior. First, there is no primary standard available at the present time for calibrating a rarefied-gas flow at supersonic velocities, so that some comparison method was necessary. Second, readings made during one run at one flow setting were not subject to errors which might occur if conditions had to be reset after the tunnel was opened and prepared for a second run. Although a static tube was used to investigate flow conditions prior to these comparison tests in order to determine approximate values of M and Re, the final data on impact-pressure corrections involved the use of impact tubes only. This precaution reduced the uncertainty due to static-pressure readings.

Four runs were made during this investigation, a run being defined as an unbroken testing period during which two of the three impact tubes were compared using one nozzle. Between runs, either nozzles or impact tubes were replaced in preparation for further tests. Chronologically, these runs involved the following combinations of nozzle and impact tubes. First, the 0.150-inch and 0.300-inch impact tubes were compared using nozzle 2. Second, the above tubes were compared in nozzle 3. Third, the 0.300-inch and the 0.600-inch impact tubes were tested in nozzle 3. Fourth, the same tubes were compared in nozzle 2.

Flow conditions corresponding to a given flowmeter setting were specified in the following manner. Each nozzle was operated over the entire range of flowmeter settings used in the investigation. At each setting of the flowmeter, measurements of pressure associated with an impact probe (14) and a static probe (15) were obtained at the test section. The impact-pressure reading combined with the Rayleigh formula gave a relation between stream Mach number M and static pressure p_s. Using the nonviscous, compressible theory for flow over a cone (reference 14), the pressure measured by the static probe yielded a relation between M and p_s. Simultaneous solution of the two equations for the two probes gave values of M and p_s. The corresponding Reynolds number was computed, with the additional assumption of the perfect gas law, as follows:

$$Re = \frac{V\rho d}{\mu}, \text{ by definition} \tag{8}$$

$$\rho = \frac{p_s}{RT} \tag{9}$$

$$M = \frac{V}{\sqrt{\gamma RT}}, \text{ by definition} \tag{10}$$

$$Re = M\sqrt{\gamma RT}\,\frac{p_s}{RT}\,\frac{d}{\mu} \tag{11}$$

Assuming adiabatic flow, the temperature T can be determined, from the measured T_o, by (reference 1)

$$T = \frac{T_o}{1 + \frac{\gamma - 1}{2} M^2} \tag{12}$$

The corresponding values of μ were determined from Sutherland's formula (reference 15)

$$\left.\begin{aligned} &\mu = \mu_o \frac{T_o + C}{T + C}\left(\frac{T}{T_o}\right)^{3/2} \\ &\mu_o = 10.0 \times 10^{-6} \text{ lb/sec-ft at } 450^\circ \text{ F absolute (reference 16)} \\ &C = 202^\circ \text{ F absolute (reference 15)} \end{aligned}\right\} \tag{13}$$

With p_s expressed in microns of mercury, T, in $^\circ$F absolute, μ, in pounds per second per foot, and the characteristic dimension d, in inches, there results

$$Re = 2.14 \times 10^{-4}\,\frac{Mp_s d}{\mu\sqrt{T}} \tag{14}$$

The Reynolds numbers computed in this manner are shown in table 1 for the conditions of the tests.

After the two corresponding impact-pressure readings were taken on the manometer for one flow condition, they were converted to pressures in microns of mercury by the calibration procedure outlined in the section "Experimental Apparatus." These data have been tabulated for all four runs in table 1. Figure 6 is a plot of the ratio of $p_{i(0.150)}$ to $p_{i(0.300)}$ against flowmeter setting for run 1. Such a plot was maintained during each run and was used as a guide to insure adequate coverage of the critical portions of the curve.

RESULTS

The impact-pressure data, together with previous knowledge of the properties of the flow at the settings used in run 1, allow the ratio of $p_{i(0.150)}$ to $p_{i(0.300)}$ to be plotted against a Reynolds number based on the small impact-tube diameter (fig. 7). The Reynolds number range covered in run 1 extended from 139 to 25 for the 0.150-inch impact tube, and from 278 to 50 for the 0.300-inch impact tube over a Mach number range of 2.8 to 2.3. Figure 7 revealed that the impact-pressure readings taken with the 0.150-inch impact tube started to vary from the impact-pressure readings taken with the 0.300-inch impact tube when the Reynolds number of the small tube was approximately 140. When the two tubes read the same impact pressure, it was assumed that this value corresponded to the pressure computed from the Rayleigh formula - $p_{i(Rayleigh)}$ - for the same flow. Since the Reynolds number value of the 0.300-inch impact tube was less than 140 during portions of run 1, it was apparent that the impact-pressure readings taken with the 0.300-inch impact tube must be corrected before a plot of the ratio of $p_{i(measured)}$ to $p_{i(Rayleigh)}$ against Reynolds number could be made. Such a correction was made using the data plotted in figure 7. Since the impact tubes were geometrically similar, it was assumed that the difference in pressure readings at a given Reynolds number for the small impact tube could be applied to the larger impact tube when the larger tube operated at the same Reynolds number. For example, in run 1, as seen in table 1, at a flowmeter setting of 79, the 0.150-inch impact tube had a Reynolds number of 71 while the 0.300-inch impact tube had a Reynolds number of 142. The difference in impact-pressure readings was 1.8 percent. Also, for a Reynolds number of 139 for the 0.150-inch impact tube and a Reynolds number of 278 for the 0.300-inch impact tube, no difference in impact-pressure readings was noted. Therefore, it was assumed that the 0.300-inch impact tube gave a pressure reading 1.8 percent higher than that of $p_{i(Rayleigh)}$ when the 0.300-inch impact tube operated at a Reynolds number of 70. This procedure gave corrected data which were plotted in figure 8 as the ratio of $p_{i(measured)}$ to $p_{i(Rayleigh)}$ against Reynolds number. The three runs following run 1 gave data which were handled in a similar manner. Figure 9 is a plot of the ratio of $p_{i(measured)}$ to $p_{i(Rayleigh)}$ against Reynolds number for all four runs.

Figures 10(a) and 10(b) are photographs of the 0.300-inch impact tube (probe 14) and the 5° half-angle static tube (probe 15). These photographs were obtained using the nitrogen-afterglow flow-visualization technique (reference 12).

Figure 11 is a plot of the impact pressures, as measured by the 0.300-inch impact tube (probe 14), at various points across the test section of nozzle 2. The figure illustrates the variation in impact-pressure distributions as flow conditions were changed.

DISCUSSION OF RESULTS

As was noted in the section "Summary of Available Analyses for Impact Tubes," reference 8 indicates that the methods of kinetic theory are applicable to interpretation of an impact tube in an extremely rarefied gas (M/Re is greater than approximately 10) and also that the continuum analysis would become invalid when the ratio $M/\sqrt{Re}$ is greater than approximately 0.01. The theories which have been advanced for the regions outside the transition range have been presented in the section mentioned above. The data gathered during these investigations cover a portion of the transition region near the estimated continuum limit $\left(0.478 > M/\sqrt{Re} > 0.165, \text{ or } 0.0929 > M/Re > 0.0083\right)$ and extend over a Mach number range of 2.3 to 3.6 and a Reynolds number range of 25 to 804.[1]

The ratio of $p_{i(measured)}$ to $p_{i(Rayleigh)}$ is plotted against $1/Re$ (fig. 12). It will be noted that the data taken with the two nozzles define two separate curves, with all points but one within ±1 percent of a faired curve drawn through the data. This one point consistently falls outside this tolerance in all plots and will be discussed later in this section. Also shown in figure 12 are two curves defined by equation (2). Points for these curves were calculated by substituting in equation (2) the suitable Mach number and Reynolds number values which were determined during the experiment. Two separate curves are defined by equation (2) because of the fact that, for a given Reynolds number, nozzle 3 produces a higher Mach number than nozzle 2.

A different picture is presented when the ratio of $p_{i(measured)}/p_{i(Rayleigh)}$ is then plotted against M/Re (fig. 13). For the purposes of comparison, the theory as defined by equation (2) is shown again and it will be noted that the theory gives two separate curves and does not correlate with M/Re although the experimental data do. A further possible correlation of the experimental data with M^2/Re (see table 1) was also made. It appeared that the correlation with M/Re

---

[1]Results of recent tests in the Ames 6-inch heat-transfer tunnel, using small spherical-head impact tubes, checked partially the basic assumption of this paper that the Rayleigh formula is applicable at the higher Reynolds numbers (300 to 800). The data, transmitted informally to the present authors, showed that no correction to the impact pressure was required for a Reynolds number of 390 and a Mach number of 2.17. These values are in agreement with the present results.

showed less scatter for the experimental points. Also, the curves obtained by using equation (2) lie more closely together when plotted as a function of M/Re rather than M^2/Re.

Examination of figures 12 and 13 indicates that the boundary-layer theory for impact tubes (reference 3) appears inadequate when used in the supersonic-flow region. Although the theory approximately predicts the point where deviations from the Rayleigh formula will start to occur, the magnitude of the deviations to be expected is not indicated by equation (2). Several reasons for this inadequacy have been proposed. First, the theory does not take into account the possible effects of slip boundary conditions which may affect impact-tube readings in this region. Second, figure 10(a), a photograph of the 0.300-inch impact tube obtained by using a nitrogen-discharge-glow technique, shows that for a Mach number of 2.4 in nozzle 2, the shock wave is approximately 0.030 inch in front of the nose of the impact tube where it may be interacting with the boundary layer. This possible interaction could well nullify the boundary-layer assumptions used in deriving this theory. Third, the boundary-layer theory is a stagnation line theory assuming a normal shock wave and does not take into account additional viscous forces which probably result from the velocity distribution behind the curved shock wave actually associated with an axially symmetric body.

It was pointed out that the magnitude of the Reynolds number was determined for each flowmeter setting by measurements with an impact probe and a static probe. The probable error in Reynolds number for any particular run is difficult to evaluate, because changes in pressure-gage calibrations, variations in ambient temperature, and errors in reading the flowmeter all contribute to the Reynolds number variation. One method of estimating the variation is to record the Reynolds number obtained during many runs for a certain flowmeter setting. For a total of approximately 20 runs with nozzle 2, extending over a period of 6 months, the maximum variation in Reynolds number was from ±6 percent at the smallest flow condition to ±4 percent at the largest flow rate. Since operational techniques, and particularly the accuracies of pressure measurements, were improved considerably when the present experiments were performed, it is reasonable to assume that the maximum uncertainty in Reynolds number due to random experimental errors does not exceed ±5 percent for nozzle 2. There were fewer data for nozzle 3, but four runs yielded variations in Reynolds number, at a fixed flow setting, extending from ±3 to ±2 percent over the operating range.

In addition to the presumably random errors affecting the accuracy of the Reynolds number determination, there were systematic effects present. The impact probe was influenced by the viscous effects that were the subject of this investigation. The lowest Reynolds number was 50 (based on the 0.300-inch probe diameter dimension) and occurred in nozzle 2; reference

to figure 9 shows that the error in p_i was 5.5 percent. Neglecting this effect gives a Reynolds number value which is too high by approximately 5 percent. This was the maximum error and was less for all other flow conditions. Reference to figure 13 shows that errors of this magnitude do not alter essentially the shape or the starting point of the impact-pressure correction curve.

The problem of interpretation of the readings of the static probe (15) remains, with respect to its use in determining the Reynolds number. Probe 15 is a 5° half-angle cone, for which the nonviscous theory gives ratios of probe pressure p_2 to static pressure p_s ranging from 1.10 to 1.23, for Mach numbers from 2.3 to 3.6. While viscous effects undoubtedly occur, probably in the form of a boundary layer which changes the pressure distribution from the "ideal" values, they would not be expected to have a large effect. A 50-percent change in the pressure increment on the cone surface would result in approximately 10-percent change in the static pressure deduced from the experimental probe pressure. No experimental or additional theoretical conclusions are available at the present time for the problem of viscous, compressible flow over a cone.

Since the measured impact pressures for the entire range of experimental variables are correlated as a function of M/Re, a single empirical equation can be deduced which represents the data, as follows:

$$\frac{p_{i(\text{measured})}}{p_{i(\text{Rayleigh})}} = \alpha\left(\frac{M}{Re}\right) + \beta\left(\frac{M}{Re}\right)^2 + \delta\left(\frac{M}{Re}\right)^3 \tag{15}$$

The constants α, β, and δ were determined, by successive approximations, from the data of figure 13 with the result:

$$\alpha = -0.80$$

$$\beta = 57.0$$

$$\delta = -370$$

for $2.3 < M < 3.6$ and $25 < Re < 804$. The curve defined by equation (15) and the designated constants is plotted in figure 13 and agrees with the experimental points within approximately ±0.5 percent. It must be emphasized that equation (15) is valid only for the range of variables covered in these tests. It cannot be assumed that higher Mach number conditions, for example, will follow equation (15) even if the ratio M/Re has the same magnitude as that in the present tests. For sufficiently small values of Re - that is, for a sufficiently rarefied gas - equation (15) clearly becomes inapplicable, since the formulation in

this case must approach the form indicated by equation (5). More extensive experimental work, covering the entire range of variables from continuum to large mean-free-path conditions, is required to establish completely the behavior of an impact tube at supersonic speeds throughout the transition zone.

It was pointed out in the first part of this section that one experimental point consistently fell approximately 3 percent from the curves drawn through the rest of the experimental data. This point was obtained during run 4 with the 0.300- and 0.600-inch impact tubes in nozzle 2. The Mach number was 2.3, the 0.300-inch impact tube had a Reynolds number of 50, and the 0.600-inch impact tube had a Reynolds number of 100. Figure 11 has been included to show the impact-pressure variation across the test section of nozzle 2 for various flowmeter settings. It is apparent from the impact-pressure profiles that at the lower flow settings, that is, at lower Mach number and Reynolds number values, viscous effects change the stream profile and diminish the useful portion of the test section. The 0.600-inch impact tube has been drawn to scale in figure 11 to show its size relationship to the impact-pressure profiles. From the relationship of the size of the 0.600-inch impact tube to the approximately constant portion of the stream profile, it may be assumed that the large impact tube can block the stream enough at the lower flowmeter settings to cause the stream conditions (as reflected in the impact pressure) to change by 3 percent. This effect did not occur with the same impact tube in nozzle 3. However, nozzle 3 produces a higher Mach number and Reynolds number for an equivalent flow setting, which may account for the fact that the one discrepancy in the data occurred only with nozzle 2 at the lowest Mach number investigated. The nozzle characteristics of nozzle 2 were checked in a supplementary run with the 0.300-inch impact tube to see if there was a possible distortion within the nozzle during run 4 which could account for this one discrepancy in the data. The supplementary run did not disclose any such distortion, and the values obtained previously were checked.

CONCLUSIONS

The magnitude of the errors resulting from application of the Rayleigh formula to the pressure measured with an impact tube in a rarefied gas has been determined experimentally. The results, obtained with source-shaped impact tubes for Mach numbers between 2.3 and 3.6 and Reynolds numbers from 25 to 804 (based on impact-probe diameter), led to the following conclusions:

1. The correction was found to be in a direction which yielded measured impact pressures higher than those which would be computed from the Rayleigh formula for the same free-stream Mach number and static pressures. This effect is in accordance with the predictions of the theory for viscous, compressible flow.

2. The flow conditions for which the correction becomes noticeable are predicted by viscous-compressible-flow theory, but the magnitude of the correction is underestimated by a factor of approximately 2 for the range of variables covered in the present investigation.

3. For the entire range of experimental conditions the data, in the form of the ratio of the measured impact pressure to that predicted by the Rayleigh formula, are correlated best as a function of the ratio of Mach number to Reynolds number. The correction does not exceed 1 percent when the ratio of Mach number to Reynolds number is less than 0.015. This figure is suggested as a tentative criterion for the limit of applicability of the Rayleigh formula in a rarefied gas. Additional experimental work is required before the validity of the correlation can be determined for Mach or Reynolds numbers outside the range of these tests.

University of California
Berkeley, Calif., February 23, 1950

REFERENCES

1. Liepmann, Hans Wolfgang, and Puckett, Allen E.: Introduction to Aerodynamics of a Compressible Fluid. John Wiley & Sons, Inc., 1947.

2. Homann, Fritz: Der Einfluss grosser Zähigkeit bei der Strömung um den Zylinder und um die Kugel. Z.f.a.M.M., Bd. 16, Heft 3, June 1936, pp. 153-164.

3. Chambré, P. L.: The Theory of the Impact Tube in a Viscous Compressible Gas. Rep. No. HE-150-50, Contract No. N7-ONR-295-Task 3, Eng. Res. Projects, Univ. of Calif., Nov. 1, 1948.

4. Chambré, P. L., and Smith, H. R.: The Impact Tube in a Viscous Compressible Gas. Rep. No. HE-150-63, Contract No. N7-ONR-295-Task 3, Eng. Res. Projects, Univ. of Calif., August 29, 1949.

5. Chambré, P. L., and Schaff, S. A.: The Theory of the Impact Tube at Low Pressures. Rep. No. HE-150-46, Contract No. N7-ONR-295-Task 3, Eng. Res. Projects, Univ. of Calif., May 17, 1948. (Also Jour. Aero. Sci., vol. 15, no. 12, Dec. 1948, pp. 735-737.)

6. Hurlbut, F. C.: An Experimental Investigation of Flow through Short Tubes for Large Molecular Mean Free Path. Rep. No. HE-150-54, Contract No. N7-ONR-295-Task 3, Eng. Res. Projects, Univ. of Calif., March 7, 1949.

7. Stalder, Jackson R., and Jukoff, David: Heat Transfer to Bodies Traveling at High Speed in the Upper Atmosphere. NACA TN 1682, 1948.

8. Tsien, Hsue-Shen: Superaerodynamics, Mechanics of Rarefied Gases. Jour. Aero. Sci., vol. 13, no. 12, Dec. 1946, pp. 653-664.

9. Schaaf, S. A., Horning, Dor. O., and Kane E. D.: Design and Initial Operation of a Low Density Supersonic Wind Tunnel. Rep. No. HE-150-62, Contract No. N7-ONR-295-Task 3, Eng. Res. Projects, Univ. of Calif., Aug. 15, 1949. (Also Heat Transfer and Fluid Mechanics Institute, A.S.M.E., 1949, pp. 223-242.

10. Emerson, D. E., and Schaff, S. A.: Performance of a Supersonic Nozzle in the Rarefied Gas Dynamics Regime. Rep. No. HE-150-72, Contract No. N7-ONR-295-Task 3, Eng. Res. Projects, Univ. of Calif., Aug. 30, 1950.

11. Schaaf, S. A., and Cyr, R. R.: Time Constants for Vacuum Gage Systems. Rep. No. HE-150-42, Contract No. N7-ONR-295-Task 3, Eng. Res. Projects, Univ. of Calif., March 31, 1948. (Also Jour. Appl. Phys., vol. 20, no. 9, Sept. 1949, pp. 860-863.)

12. Kane, E. D.: Preliminary Report on an Electrical Discharge Method for Flow Visualization in a Low Density Supersonic Wind Tunnel. Rep. No. HE-150-51, Contract No. N7-ONR-295-Task 3, Eng. Res. Projects, Univ. of Calif., Feb. 23, 1949.

13. Williams, Thomas W., and Benson, James M.: Preliminary Investigation of the Use of Afterglow for Visualizing Low-Density Compressible Flows. NACA TN 1900, 1949.

14. Staff of the Computing Section (under the direction of Zdenek Kopal): Tables of Supersonic Flow around Cones. Tech. Rep. No. 1, Center of Analysis, M.I.T., 1947.

15. National Research Council (Edward W. Washburn, ed.): International Critical Tables. Vol. V. First ed., McGraw-Hill Book Co., Inc., 1929.

16. Keenan, Joseph Henry, and Kaye, Joseph: Thermodynamic Properties of Air including Polytropic Functions. John Wiley & Sons, Inc., 1945.

TABLE 1.- EXPERIMENTAL DATA

Run	Flow-meter setting (1)	Tube diameter (in.)	Re (per in.)	Re	M	p_i(measured) (microns of mercury)	$\frac{p_i(0.150)}{p_i(0.300)}$	$\frac{p_i(\text{measured})}{p_i(\text{Rayleigh})}$	$\frac{1}{Re}$	$\frac{M}{Re}$	$\frac{M^2}{Re}$
1 (nozzle 2)	21.5(LF)	0.300	930	278	2.8	1255	0.995	1.000	0.36×10^{-2}	0.99×10^{-2}	2.7×10^{-2}
	21.5(LF)	.150	930	139	2.8	1250		.995	.72	1.98	5.4
	79	.300	480	142	2.45	710	1.018	1.000	.71	1.7	4.2
	79	.150	480	71	2.45	722		1.018	1.42	3.4	8.4
	50	.300	340	100	2.4	513	1.045	1.005	1.0	2.4	5.7
	50	.150	340	50	2.4	536		1.050	2.0	4.8	11.4
	30	.300	240	71	2.35	380	1.062	1.018	1.4	3.3	7.7
	30	.150	240	35.5	2.35	404		1.080	2.8	6.6	15.4
	18	.300	170	50	2.3	265	1.082	1.050	2.0	4.6	11.0
	18	.150	170	25	2.3	287		1.130	4.0	9.2	22.0
2 (nozzle 3)	28 (LF)	0.300	1830	550	3.6	1930	0.999	1.000	0.18	0.65	4.6
	28 (LF)	.150	1830	275	3.6	1928		.999	.36	1.30	9.2
	22 (LF)	.300	1340	402	3.3	1601	1.000	1.000	.25	.83	2.8
	22 (LF)	.150	1340	201	3.3	1602		1.000	.50	1.66	5.6
	130	.300	1120	336	3.25	1359	1.005	1.000	.30	.98	3.2
	130	.150	1120	168	3.25	1367		1.005	.60	1.96	6.4
	100	.300	960	288	3.2	1061	1.007	1.000	.35	1.1	3.6
	100	.150	960	144	3.2	1069		1.007	.70	2.2	7.2
	72	.300	870	262	3.45	931	1.011	1.000	.38	1.3	4.5
	72	.150	870	131	3.45	942		1.011	.76	2.6	9.0
	56	.300	640	192	3.1	787	1.023	1.000	.52	1.6	5.0
	56	.150	640	96	3.1	805		1.023	1.04	3.2	10.0
	40	.300	490	148	2.9	635	1.042	1.000	.68	2.0	5.8
	40	.150	490	74	2.9	661		1.042	1.36	4.0	11.6
	30	.300	390	118	2.8	547	1.045	1.011	.85	2.4	6.7
	30	.150	390	59	2.8	571		1.057	1.70	4.8	13.4
	20	.300	340	102	3.0	430	1.049	1.022	.99	2.9	8.7
	20	.150	340	51	3.0	451		1.068	1.98	5.8	17.4
	14	.300	230	70	2.8	332	1.070	1.045	1.4	4.0	11.0
	14	.150	230	35	2.8	355		1.120	2.8	8.0	22.0
3 (nozzle 3)	22 (LF)	0.600	1340	804	3.3	1618	0.996	1.000	0.12	0.42	1.4
	22 (LF)	.300	1340	402	3.3	1610		.996	.24	.84	2.8
	130	.600	1120	672	3.25	1366	.998	1.000	.15	.49	1.6
	130	.300	1120	336	3.25	1364		.998	.30	.98	3.2
	100	.600	960	576	3.2	1174	.993	1.000	.17	.56	1.8
	100	.300	960	288	3.2	1166		.993	.34	1.12	3.6
	72	.600	870	524	3.45	937	1.006	1.000	.19	.66	2.3
	72	.300	870	262	3.45	942		1.006	.38	1.32	4.6
	56	.600	640	384	3.1	783	1.009	1.000	.26	.81	2.5
	56	.300	640	192	3.1	790		1.009	.52	1.62	5.0
	40	.600	490	296	2.9	635	1.010	1.000	.34	.99	2.9
	40	.300	490	148	2.9	641		1.010	.68	1.98	5.8
	30	.600	390	236	2.8	534	1.010	1.000	.42	1.2	3.3
	30	.300	390	118	2.8	539		1.010	.84	2.4	6.6
	20	.600	340	204	3.0	417	1.025	1.000	.50	1.4	4.3
	20	.300	340	102	3.0	427		1.025	1.00	2.8	8.6
	14	.600	230	140	2.8	328	1.040	1.005	.72	2.0	5.7
	14	.300	230	70	2.8	341		1.045	1.44	4.0	11.4
4 (nozzle 2)	21.5(LF)	0.600	930	556	2.8	1235	1.007	1.000	0.18	0.50	1.4
	21.5(LF)	.300	930	278	2.8	1232		1.007	.36	1.0	2.8
	79	.600	480	284	2.45	693	.995	1.000	.36	.86	2.1
	79	.300	480	142	2.45	689		.995	.72	1.7	4.2
	50	.600	340	200	2.4	505	1.018	1.000	.50	1.2	2.9
	50	.300	340	100	2.4	515		1.018	1.00	2.4	5.9
	30	.600	240	142	2.35	400	1.026	1.000	.71	1.6	3.9
	30	.300	240	71	2.35	410		1.026	1.42	3.2	7.7
	18	.600	170	100	2.3	258	1.084	1.018	1.0	2.3	5.4
	18	.300	170	50	2.3	280		1.102	2.0	4.6	10.8

[1]Abbreviation LF refers to larger float; undesignated readings apply to smaller float.

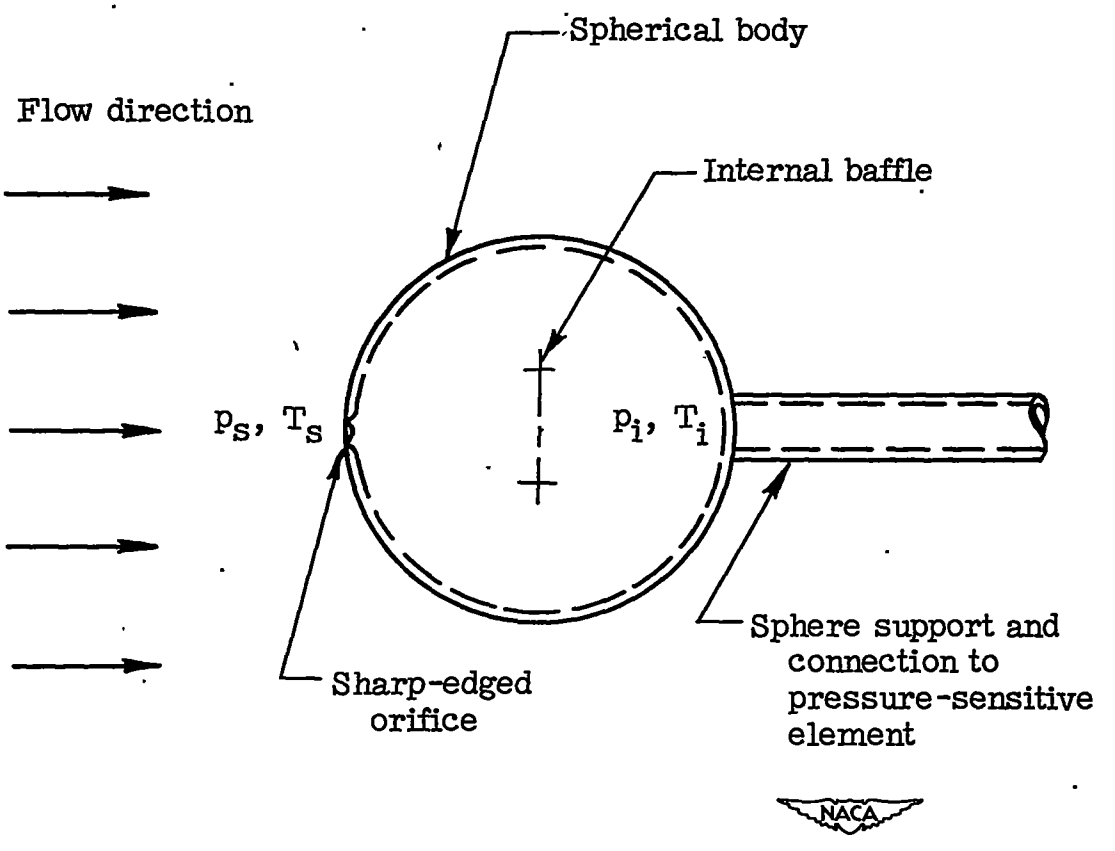

Figure 1.- Schematic diagram of spherical impact tube.

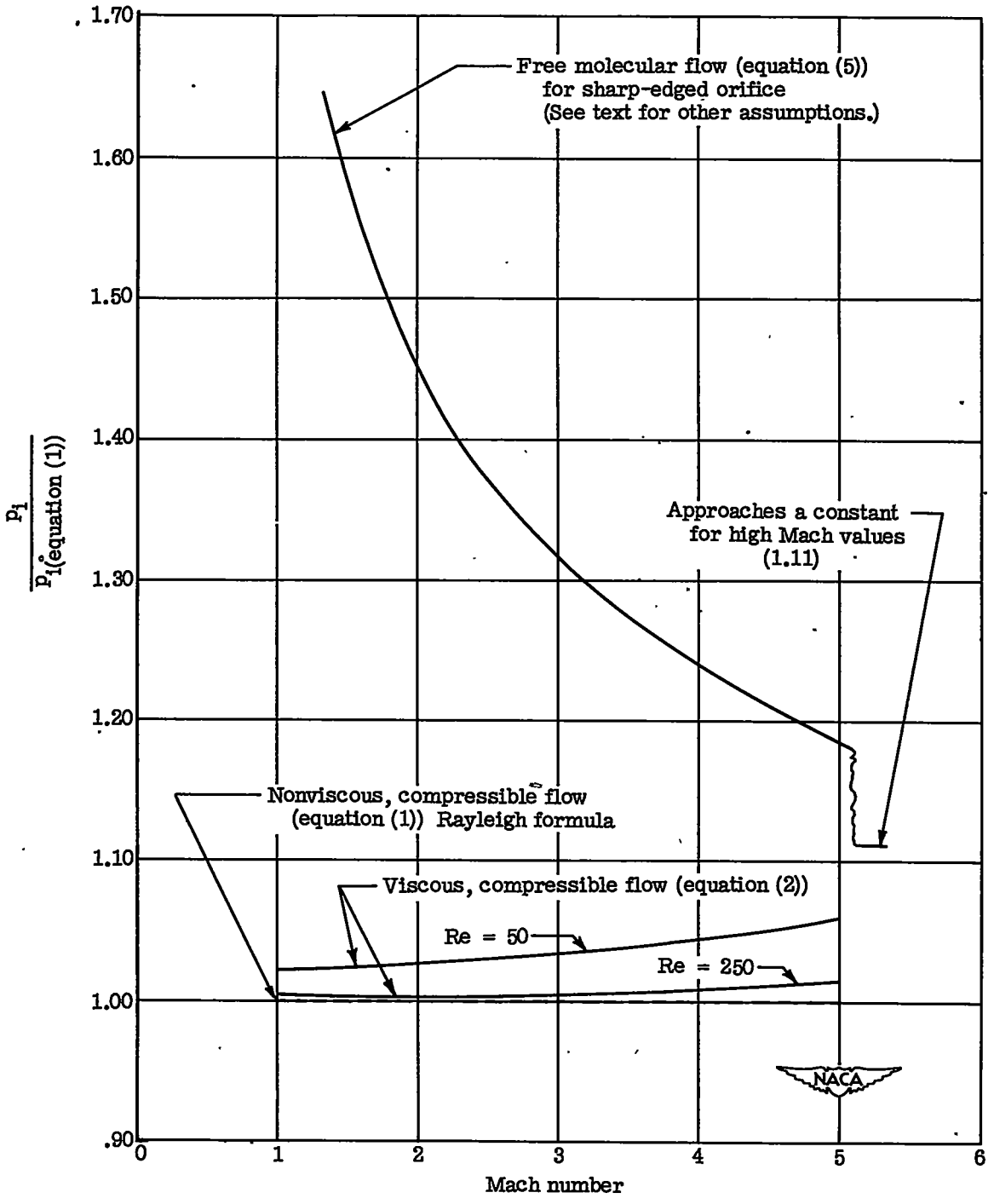

Figure 2.- Comparison of theoretical impact-tube equations. Spherical probe in air.

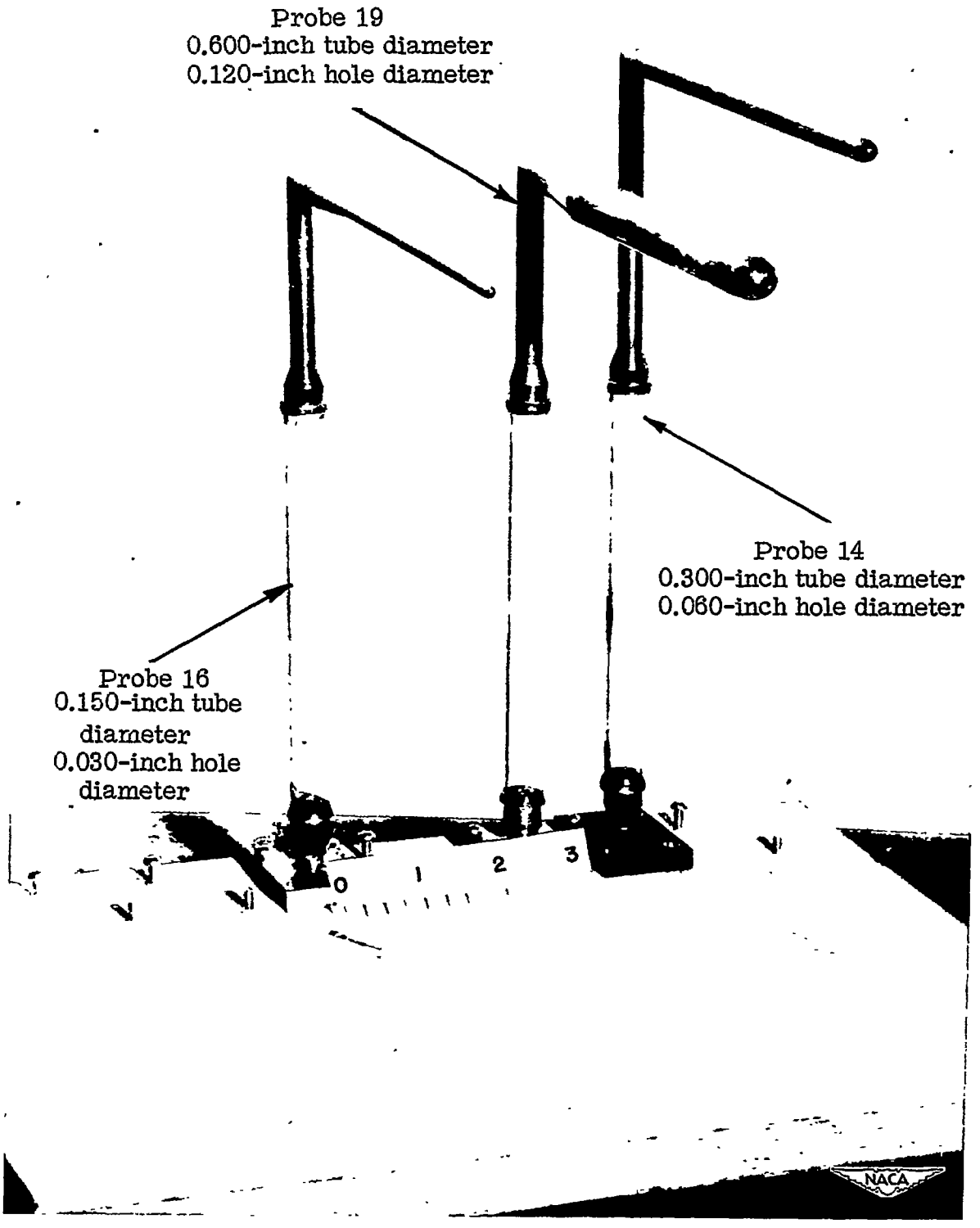

Figure 3.- Impact tubes used in investigation.

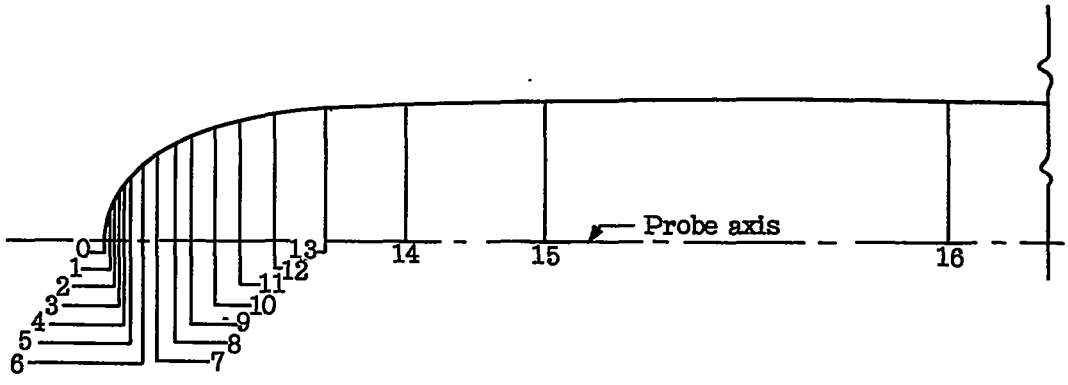

Station	Probe 14 0.300-inch tube diameter 0.060-inch hole diameter[1]		Probe 16 0.150-inch tube diameter 0.030-inch hole diameter[1]		Probe 19 0.600-inch tube diameter 0.120-inch hole diameter[1]	
	Axial distance	Offset	Axial distance	Offset	Axial distance	Offset
0	0	0	0	0	0	0
1	.0054	.0325	.0027	.0163	.0108	.0650
2	.0076	.0389	.0038	.0195	.0152	.0778
3	.0139	.0513	.0070	.0257	.0278	.1026
4	.0219	.0634	.0110	.0317	.0438	.1268
5	.0317	.0750	.0159	.0375	.0634	.1500
6	.0437	.0860	.0219	.0430	.0874	.1720
7	.0580	.0964	.0290	.0482	.1160	.1928
8	.0750	.1061	.0375	.0531	.1500	.2122
9	.0953	.1149	.0477	.0575	.1906	.2298
10	.1197	.1229	.0599	.0615	.2394	.2458
11	.1500	.1299	.0750	.0650	.3000	.2598
12	.1891	.1359	.0946	.0680	.3782	.2718
13	.2429	.1410	.1215	.0705	.4858	.2820
14	.3260	.1449	.1630	.0725	.6520	.2898
15	.4808	.1477	.2404	.0739	.9616	.2954
16	.9224	.1494	.4612	.0747	1.8448	.2988

[1]Hole in probe to be bored after tube is formed according to above offsets.

Figure 4.- Profile data for source-shaped impact tubes.

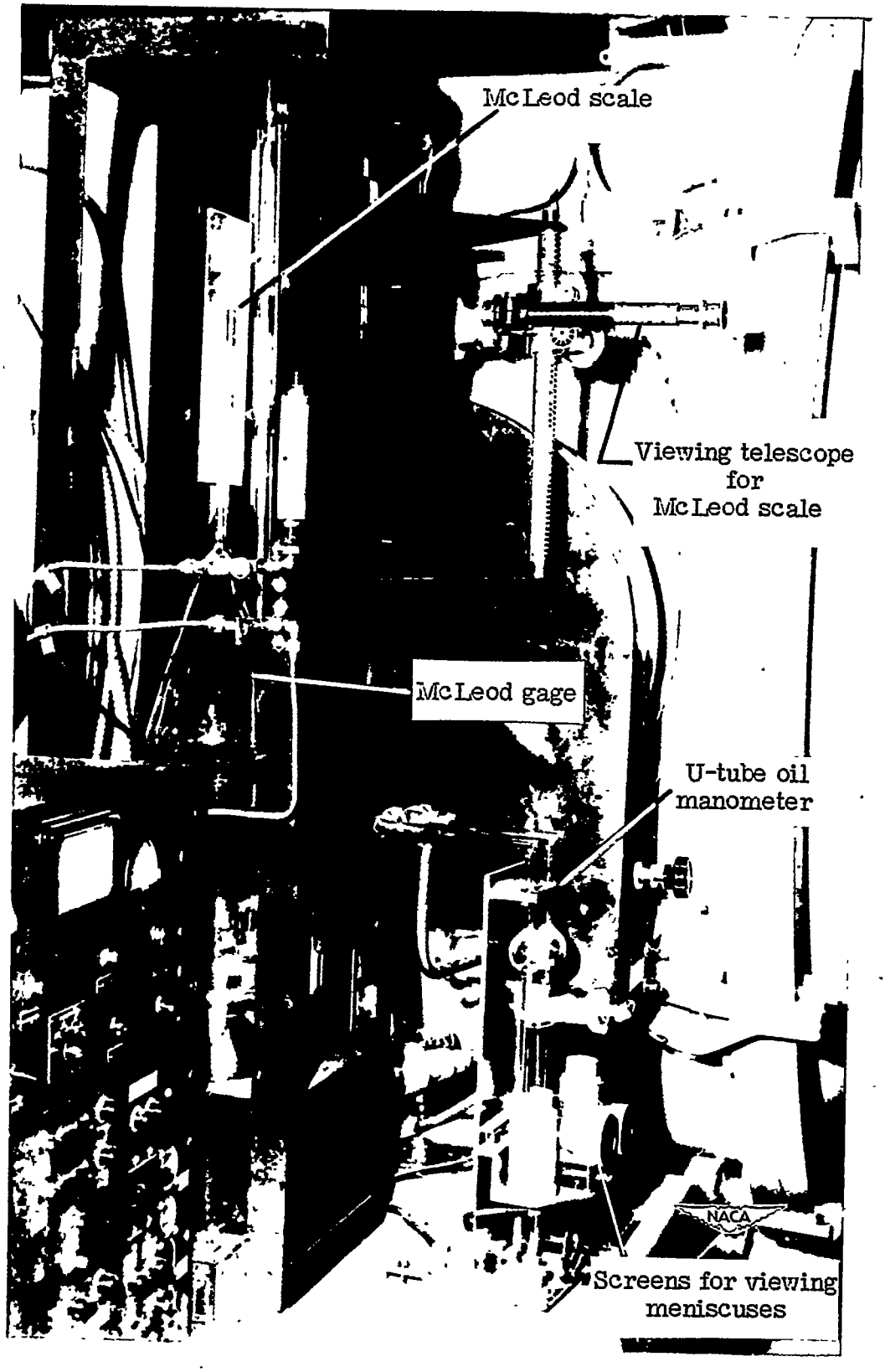

Figure 5.- U-tube oil manometer and McLeod gages.

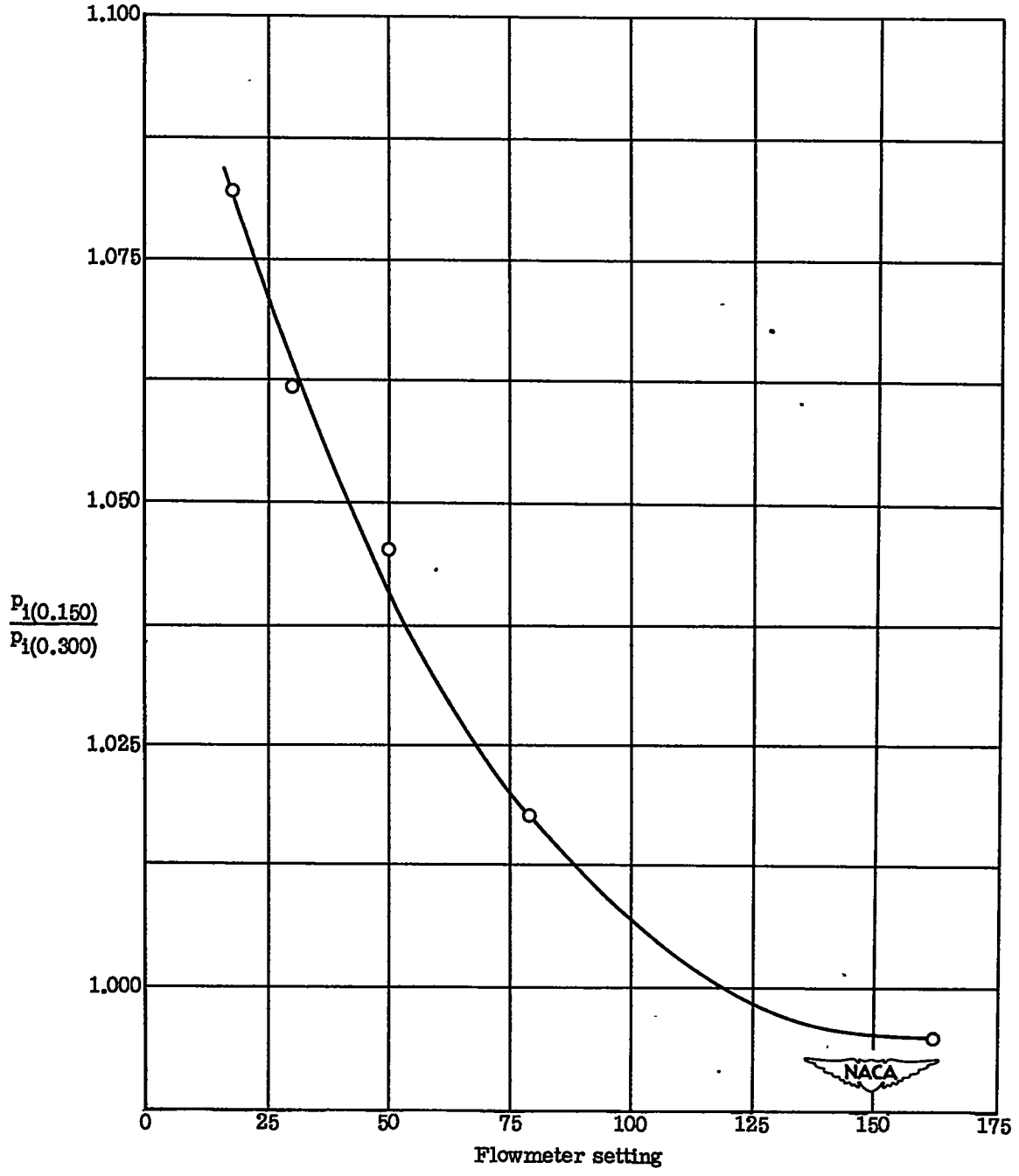

Figure 6.- The ratio $\frac{p_{i(0.150)}}{p_{i(0.300)}}$ against flowmeter setting. Run 1.

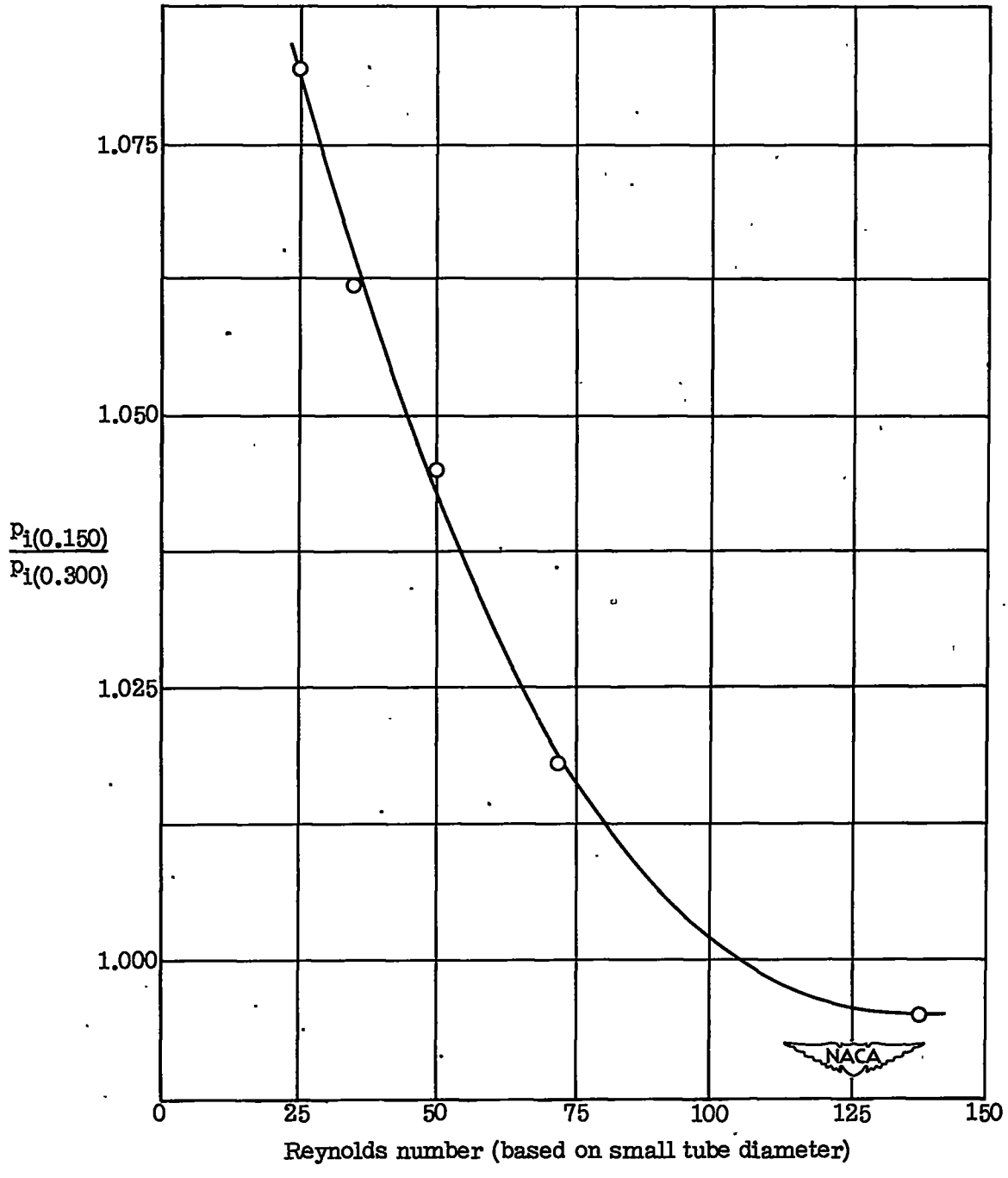

Figure 7.- The ratio $\frac{p_{i(0.150)}}{p_{i(0.300)}}$ against Reynolds number (based on small tube diameter). Run 1.

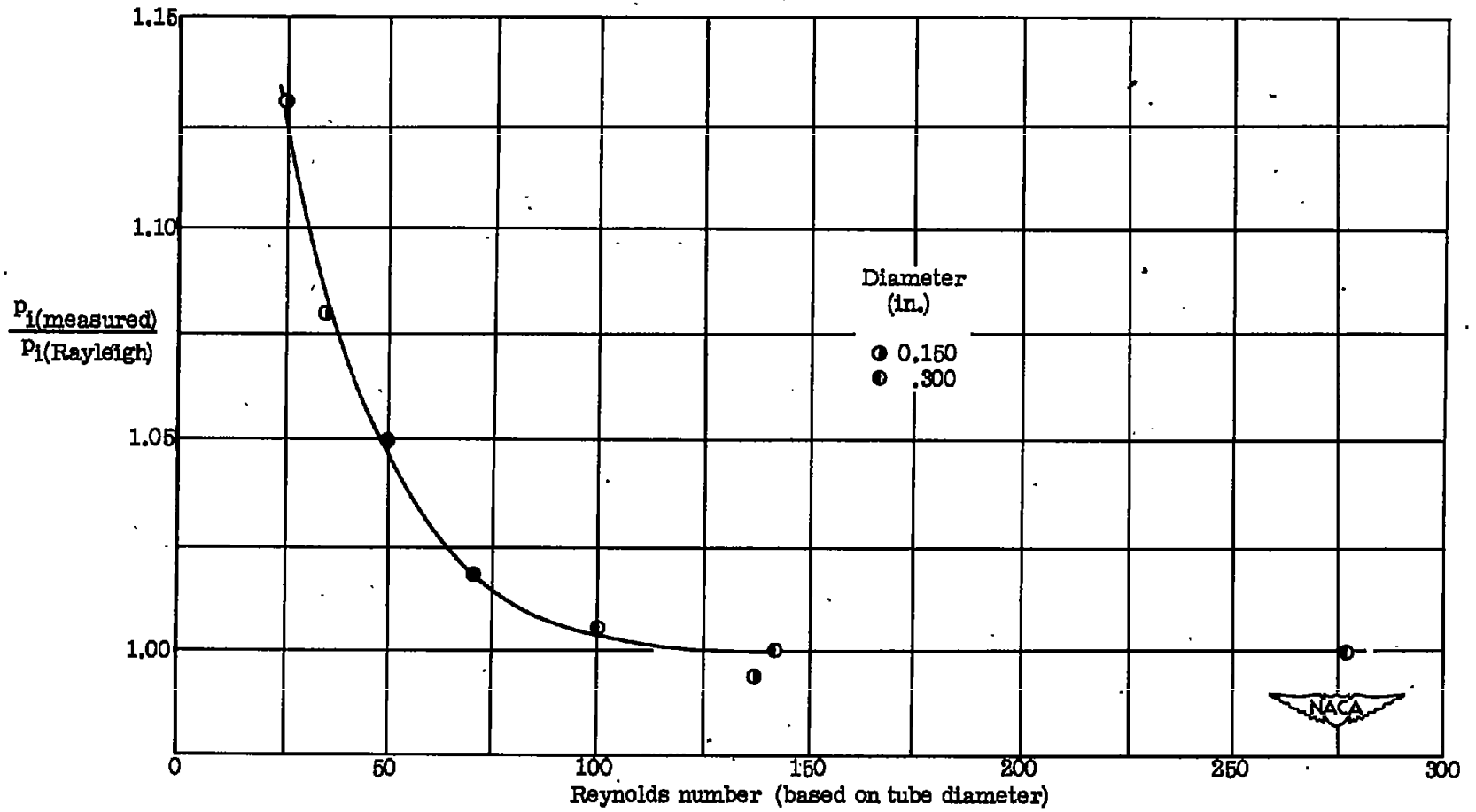

Figure 8.- The ratio $\frac{p_{i(measured)}}{p_{i(Rayleigh)}}$ against Reynolds number (based on tube diameter). Run 1.

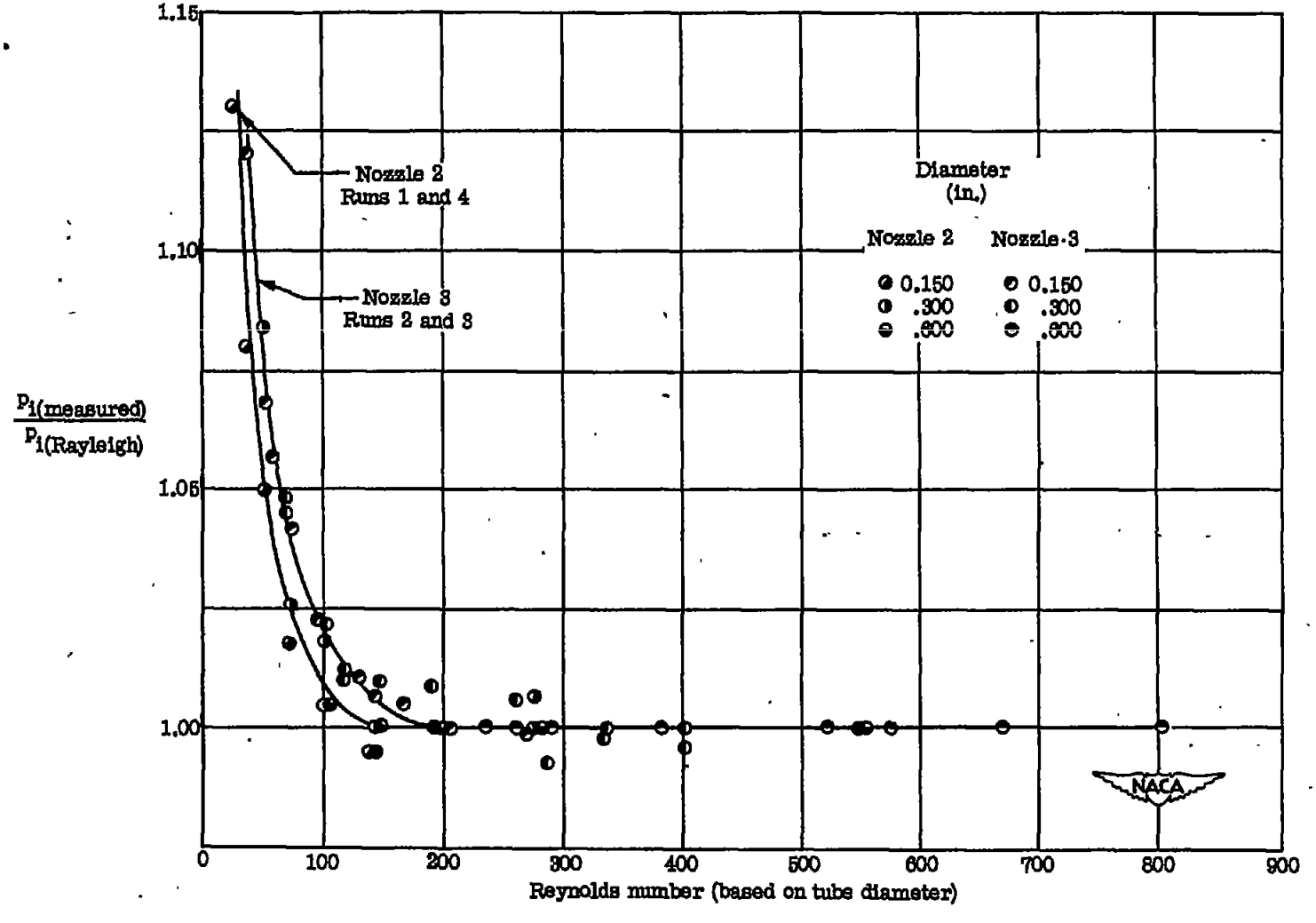

Figure 9.- The ratio $\frac{p_{i(measured)}}{p_{i(Rayleigh)}}$ against Reynolds number (based on tube diameter).

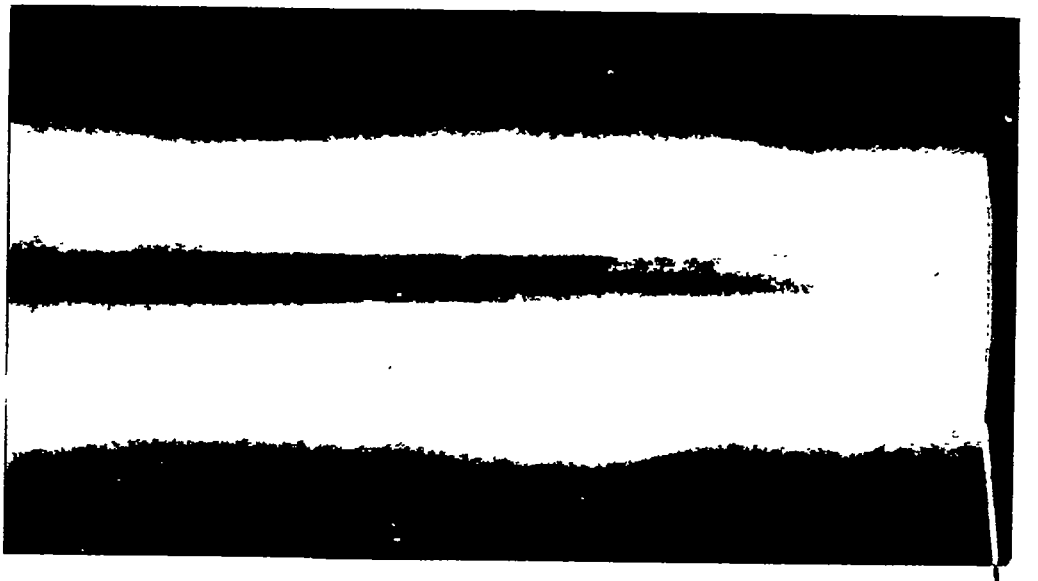

(a) Probe 14.

Edge of nozzle

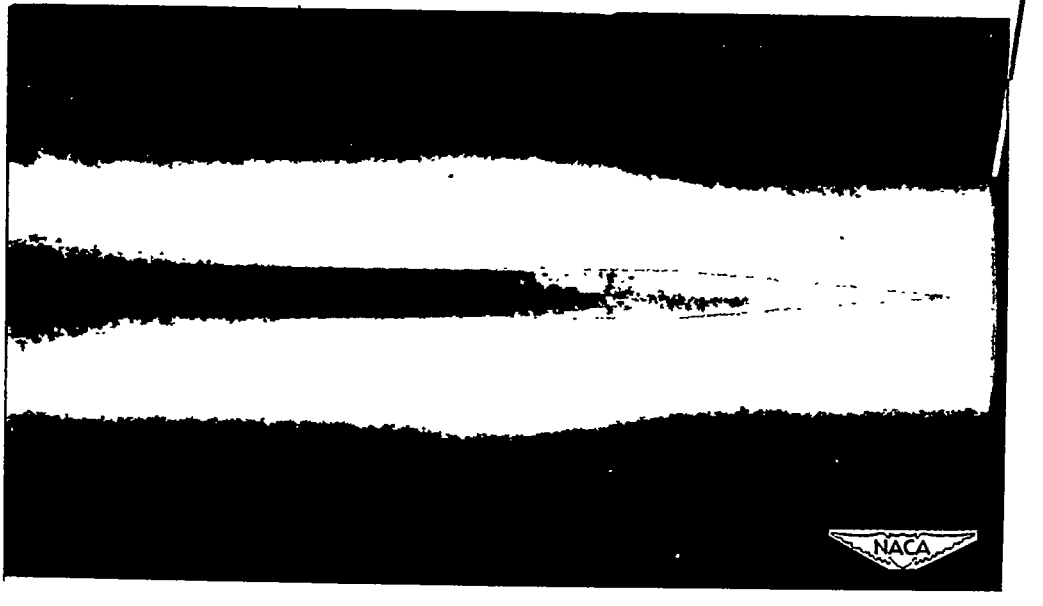

(b) Probe 15.

Figure 10.- Photographs of 0.300-inch impact tube (probe 14) and 5° half-angle static tube (probe 15). Gas used, nitrogen; flowmeter setting, 80; Re, 480 (per inch); M, 2.4. (Scale, approx. five-sixths full size).

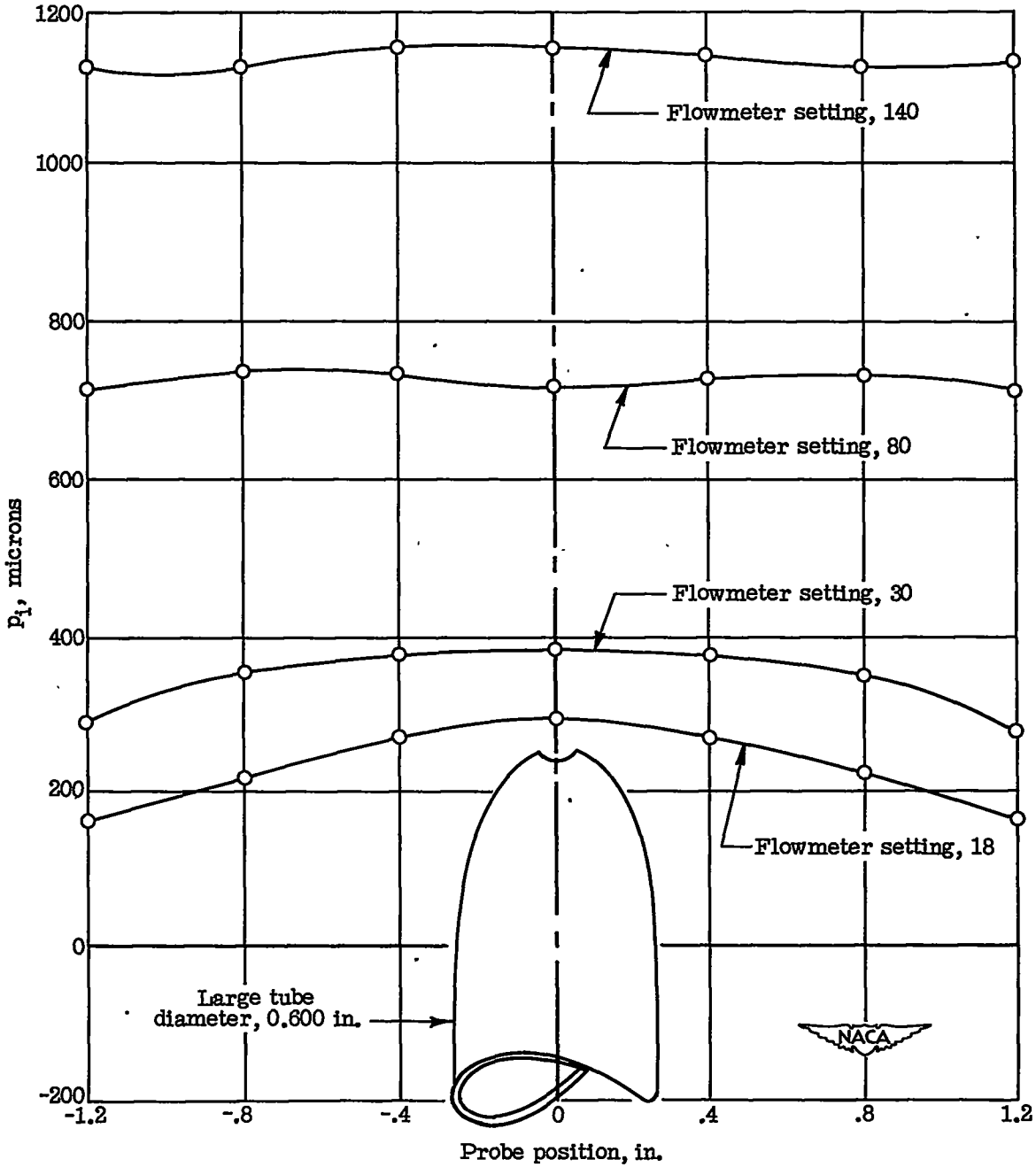

Figure 11.- Impact-pressure profiles. Nozzle 2.

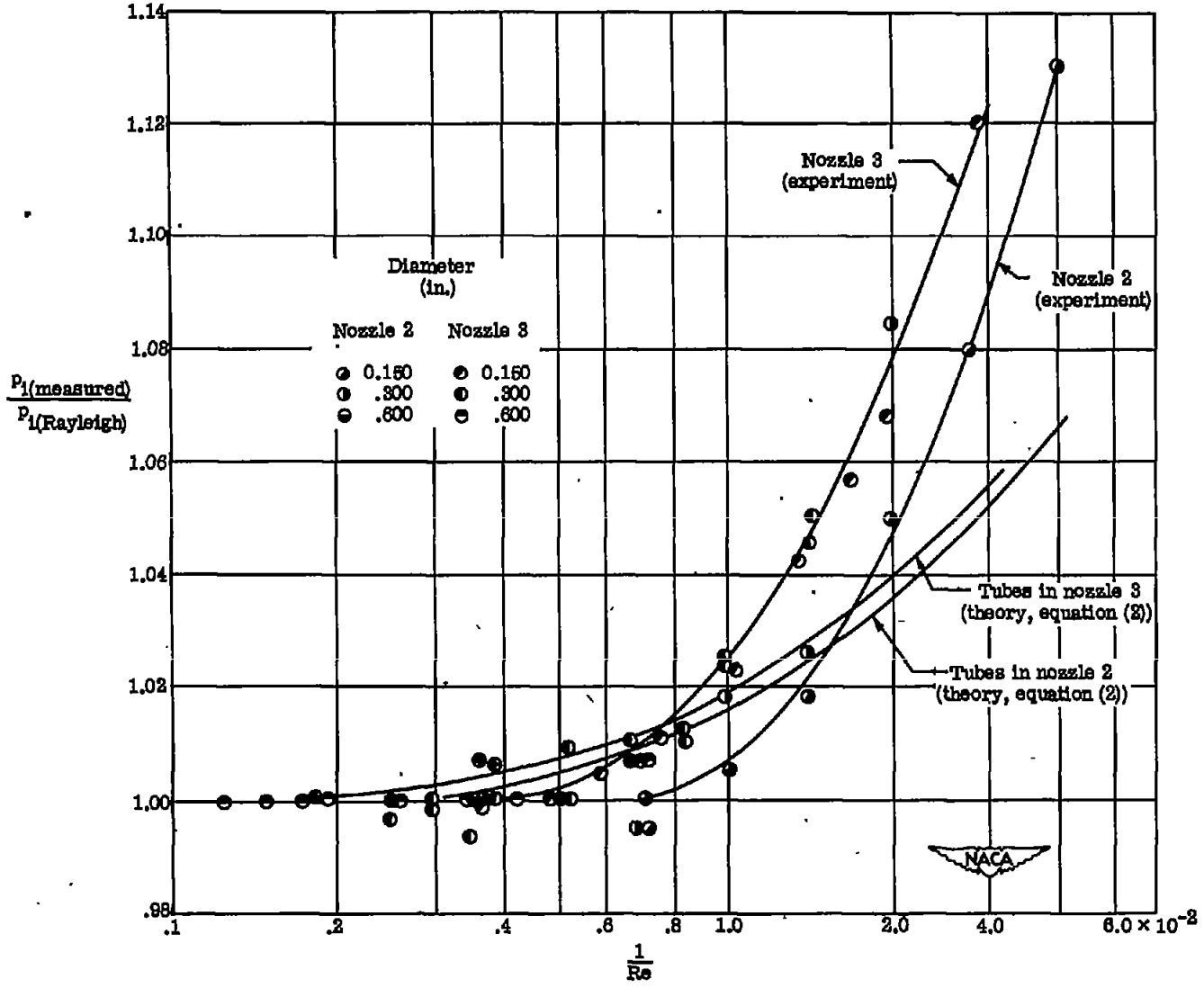

Figure 12.- The ratio $\frac{p_{i(measured)}}{p_{i(Rayleigh)}}$ against $\frac{1}{Re}$. $2.3 < M < 3.6$; $25 < Re < 804$.

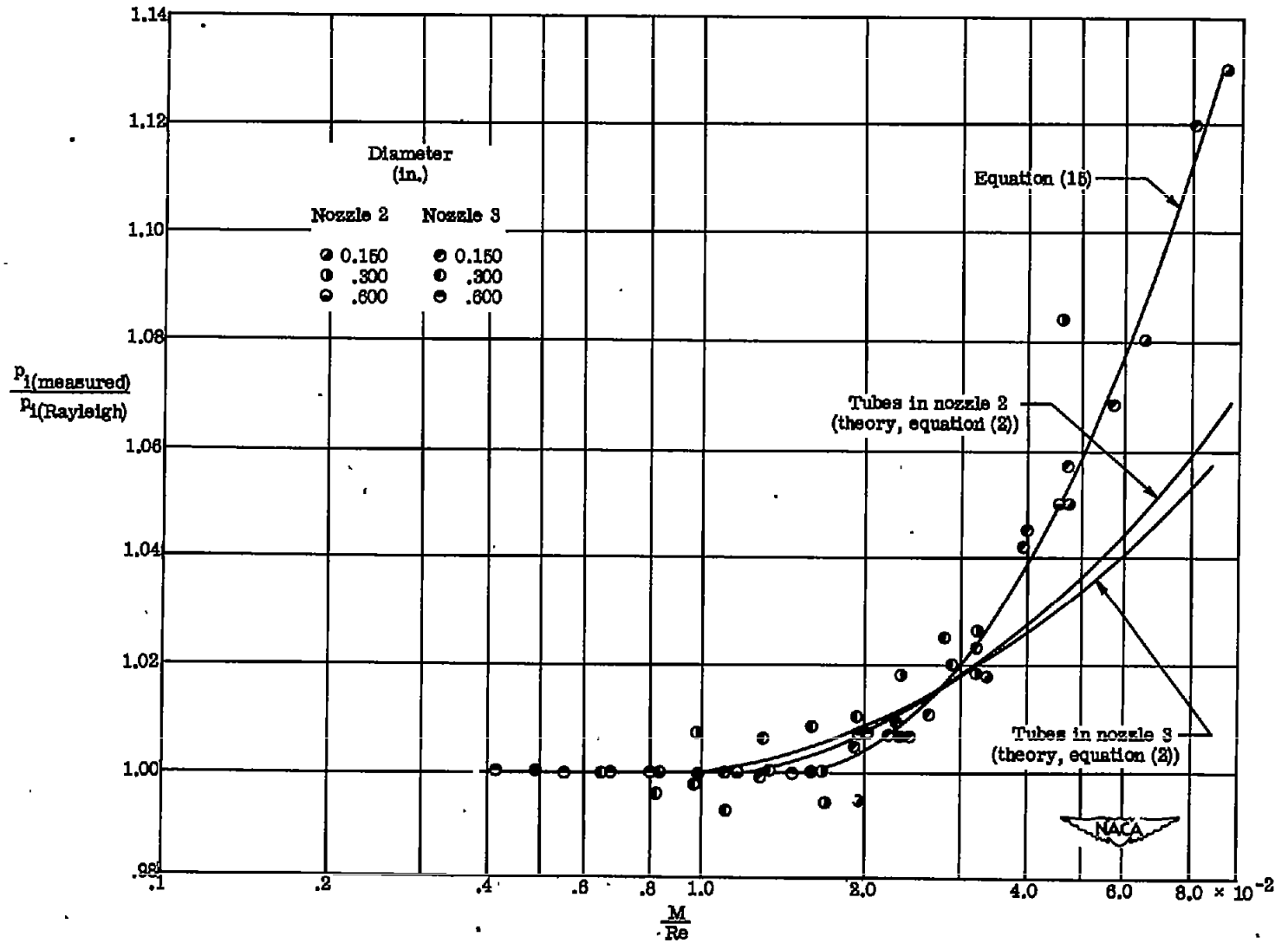

Figure 13.- The ratio $\frac{p_{i(measured)}}{p_{i(Rayleigh)}}$ against $\frac{M}{Re}$. $2.3 < M < 3.6$; $25 < Re < 804$.

NACA-Langley - 10-28-50 - 1125